

Domain-wall pinning, nonadiabatic spin-transfer torque, and spin-current polarization in permalloy wires doped with vanadium

S. Lepadatu,¹ J. S. Claydon,¹ C. J. Kinane,² T. R. Charlton,² S. Langridge,² A. Potenza,³ S. S. Dhesi,³ P. S. Keatley,⁴ R. J. Hicken,⁴ B. J. Hickey,¹ and C. H. Marrows¹

¹*E.C. Stoner Laboratory, School of Physics and Astronomy, University of Leeds, Leeds LS2 9JT, United Kingdom*

²*Rutherford Appleton Laboratory, ISIS, Chilton, Didcot OX11 0QX, United Kingdom*

³*Diamond Light Source, Chilton, Didcot OX11 0DE, United Kingdom*

⁴*School of Physics, University of Exeter, Exeter EX4 4QL, United Kingdom*

(Received 26 October 2009; published 29 January 2010)

Using pulsed-current measurements we investigate the domain-wall depinning via spin-transfer torque from pinning potentials in V-doped Ni₈₀Fe₂₀ wires. The domain-wall depinning boundary, showing the variation of threshold current density with longitudinal magnetic field is measured and reproduced using micromagnetic simulations. This method allows us to determine the spin-current polarization and nonadiabaticity parameter in these materials. By increasing the V concentration we show that the nonadiabaticity parameter is increased while the Gilbert damping is unaffected. On the other hand the spin-current polarization is decreased, resulting in larger threshold current densities.

DOI: [10.1103/PhysRevB.81.020413](https://doi.org/10.1103/PhysRevB.81.020413)

PACS number(s): 72.25.Ba, 72.25.Pn, 75.60.Ch

The ability to manipulate domain walls in magnetic materials by applying electrical currents¹ is of great interest for spintronics devices, such as magnetic memory devices.² The mechanism responsible for the interaction between spin-polarized currents and domain walls is called the spin-transfer torque effect.³ The spin torques acting on a domain wall are composed of two terms, namely, the adiabatic⁴ and the nonadiabatic^{5,6} spin torques, with the latter being proportional to a material-dependent constant β known as the nonadiabaticity parameter. A number of recent studies have investigated the contribution of the nonadiabatic spin torque in various materials and systems.^{7–9} The relationship between the two phenomenological constants representing dissipative effects β and the Gilbert damping constant α has also come under debate with theoretical arguments given for both the cases of $\beta \neq \alpha$ (Ref. 10) and $\beta = \alpha$.¹¹ We have recently demonstrated a method to measure the spin-current polarization and nonadiabaticity parameter in Ni₈₀Fe₂₀.^{12,13} Since the threshold current required to move or depin a domain wall depends on the value of β , methods of controlling the nonadiabatic spin torque are of particular importance. According to theoretical formulations β is inversely proportional to the spin-flip lifetime of conduction electrons.⁶ In a recent work on PtCo layers, another method of determining the contribution of the nonadiabatic spin torque has been demonstrated.¹⁴ By introducing an AlO_x layer to break the symmetry properties and increase the spin-flip rate, an enhanced spin-torque effect compared to the symmetric PtCoPt structure was shown. In this work we investigate the possibility of modifying β by introducing impurities in Ni₈₀Fe₂₀. The impurities act as scattering centers for the conduction electrons, reducing the spin-flip lifetimes and thus increasing the value of β . Moreover, since the damping in Ni₈₀Fe₂₀ is known to be largely unaffected by V doping up to 10% concentration,¹⁵ this experiment also allows us to investigate the relationship between β and α .

Notched wires were fabricated on Si/SiO₂ substrates using *e*-beam lithography. The material is deposited using sput-

tering of V-doped Py (Py=Ni₈₀Fe₂₀) targets, Py₉₉V₁, Py_{97.5}V_{2.5}, and Py₉₀V₁₀ respectively, with 20 nm thickness and a 1.5 nm thick Al capping layer. The wires were patterned with an elliptical nucleation pad and a 31° linear pinning potential as described previously.^{12,13} The wire width was 1 μm and the constriction width was 100 nm. The elliptical pad was used to nucleate a domain wall after reversal from saturation. Thus, the wire was saturated with a longitudinal magnetic field (i.e., along the axis of the wire) of magnitude greater than 700 Oe, following which a reverse field of 10 Oe is applied, resulting in a domain wall being injected into the wire from the elliptical nucleation pad and trapped at the pinning potential. The structure of the domain wall pinned at the notch was investigated by means of x-ray magnetic circular dichroism photoemission electron microscopy (PEEM) imaging with the I06 beamline at the Diamond Light Source synchrotron. Imaging was carried out at nominally zero field (less than 1 Oe), after saturation in 700 Oe and the application of a 10 Oe reverse field to nucleate and propagate the wall to the notch. Circularly polarized x-ray photons with energies corresponding to the Fe L₃ and L₂ absorption edges have been used. Typical PEEM images of the wires under study are shown in Fig. 1 for the three different V concentrations. We find that a transverse domain wall is pinned at the center of the pinning potentials in all cases, as in the case of pure Py.¹²

In order to simulate the domain-wall depinning characteristics, we next measure the material parameters relevant for a micromagnetic description of these systems. Py₉₉V₁, Py_{97.5}V_{2.5}, and Py₉₀V₁₀ thin films have been sputtered with 20 nm thickness on Si/SiO₂ substrates. Figure 2(a) shows a set of vibrating sample magnetometer (VSM) measurements for the V-doped Py and pure Py films, where the normalized saturation magnetization is plotted as a function of temperature. The experimental points are fitted using the Bloch law $M_S = (m_S/m_0) = 1 - cT^{3/2}$ in order to obtain the exchange stiffness constant values A . For these films we have the relation $A = 4.22 \times 10^8 k_B/c^{2/3}$,¹⁶ and we obtain $A = 1.2 \times 10^{-11}$ J/m

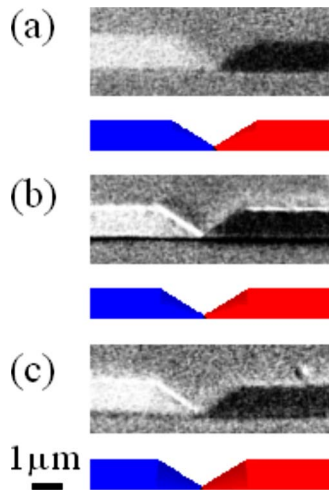


FIG. 1. (Color online) PEEM images and micromagnetic simulations showing equilibrium pinning states for a domain wall in (a) Py_{99}V_1 , (b) $\text{Py}_{97.5}\text{V}_{2.5}$, and (c) $\text{Py}_{90}\text{V}_{10}$.

for Py_{99}V_1 , $A=9.7 \times 10^{-12}$ J/m for $\text{Py}_{97.5}\text{V}_{2.5}$, and $A=6 \times 10^{-12}$ J/m for $\text{Py}_{90}\text{V}_{10}$. Moreover, the saturation magnetization values at room temperature are obtained as $m_S=850 \times 10^3$ A/m for Py_{99}V_1 , $m_S=840 \times 10^3$ A/m for $\text{Py}_{97.5}\text{V}_{2.5}$, and $m_S=770 \times 10^3$ A/m for $\text{Py}_{90}\text{V}_{10}$. For pure Py we have the usual values $A=1.3 \times 10^{-11}$ J/m and $m_S=860 \times 10^3$ A/m at room temperature. The effect of V

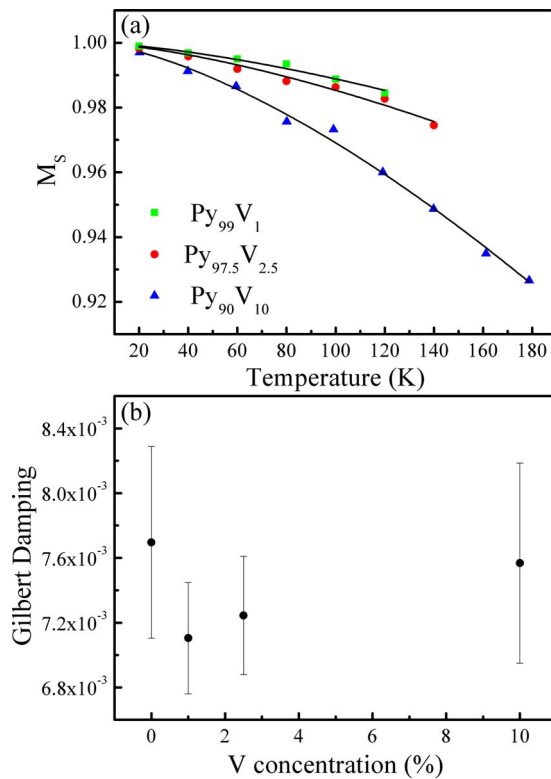


FIG. 2. (Color online) (a) VSM measurements of 20 nm V-doped permalloy thin films with Bloch law fits showing normalized saturation magnetization as a function of temperature and (b) Gilbert damping parameter as a function of V concentration in 20 nm V-doped thin films, showing experimental error margins.

doping on the magnetic properties of Ni films has been studied previously.¹⁷ It was shown that both the Curie temperature and zero-temperature magnetization markedly decrease as the concentration of V is increased, similar to our observation here in Py.

The magnetocrystalline anisotropy of these films has been characterized using longitudinal magneto-optical Kerr effect (MOKE) measurements. For all the V concentrations up to 10% the films have a small uniaxial magnetocrystalline anisotropy with negligible anisotropy constant when compared with the shape anisotropy of the wires. We have also determined the Gilbert damping constant α in these films, using time-resolved MOKE (TR-MOKE) measurements following excitation by a field pulse.^{18,19} Magnetization precession around an in-plane bias field H was excited by an in-plane field pulse perpendicular to H and the magnetization precession was detected using a polar TR-MOKE setup. For the case of negligible in-plane and no out-of-plane anisotropy, as is the case of our V-doped thin films, the Gilbert damping constant is obtained as $\alpha=1/\gamma\tau(H+m_S/2)$,¹⁶ where $\gamma=2.21 \times 10^5$ m/A s is the gyromagnetic ratio and τ is the decay time constant obtained from the measured magnetization precession. Using bias fields of 300 and 380 Oe we obtained the values of α as a function of the V concentration. For the two bias fields used the values of α agree within the experimental error margin, and the average of the two values is shown in Fig. 2(b) as a function of the V concentration. We find that within the experimental error margins the values of α are independent of the V concentration. This is in agreement with previous studies of Gilbert damping as a function of V doping using ferromagnetic resonance measurements.¹⁵

The structure of the pinned domain walls was investigated by micromagnetic simulations using the object-oriented micromagnetic framework (OOMMF) code²⁰ with the parameters determined above for the various V concentrations. A vortex domain wall was introduced in the left-hand side of the notch and the system is left to relax in a 10 Oe longitudinal magnetic field. After the system achieves a stable state (stopping condition of $|m \times H|/m_S^2 < 10^{-5}$), the magnetic field is set to zero and the system is relaxed again to obtain the final state. The stable domain-wall pinning positions are shown in Fig. 1, compared to the pinning positions obtained from the PEEM imaging. A good agreement between the PEEM images and simulations is found, showing a transverse domain wall pinned at the center of the notch.

To allow for pulsed-current measurements the wires were contacted with Ti (10 nm)/Au (140 nm) pads. Current pulses were applied to the wires using an impedance matched probe in contact with the pads, while the resistance was measured using a lock-in amplifier as described previously.^{12,13} Since the anisotropic magnetoresistance associated with a domain wall results in a decreased resistance, the pinning and depinning of a domain wall from the notch are detected by measuring the resistance state of the wires. Following domain-wall pinning at the notch a longitudinal magnetic field between 0 and 14 Oe was set and a current pulse of 300 ns width and set amplitude were applied. By varying the current pulse amplitude and magnetic field, the threshold depinning current is measured as a function of longitudinal magnetic field. The resulting depinning boundaries are shown in Fig.

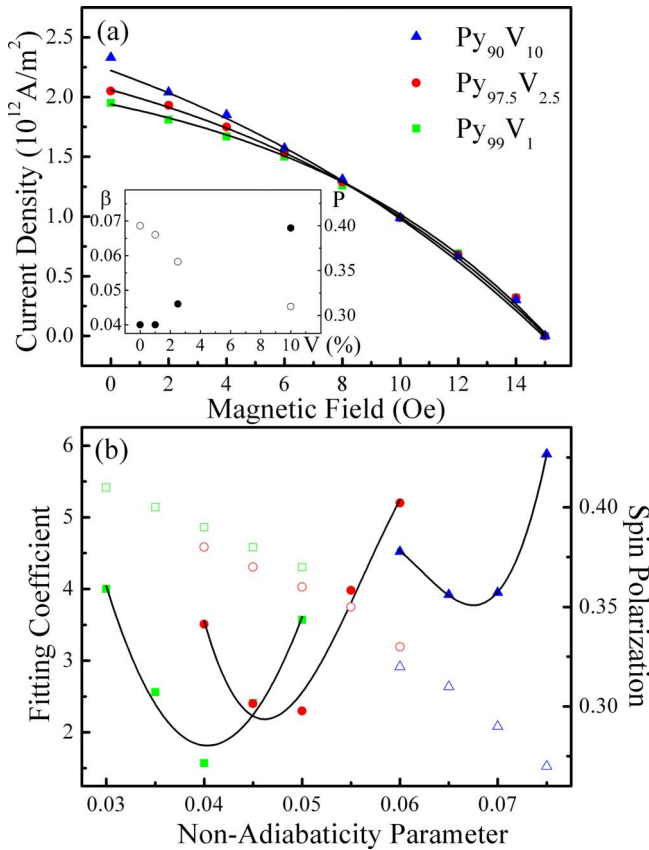


FIG. 3. (Color online) (a) Experimental depinning boundaries for V-doped permalloy wires (points) and best-fit simulated depinning boundaries, respectively (solid lines). In the inset β (solid circles) and P (empty circles) are plotted as functions of V content. (b) Fitting coefficients (solid points) and best-fit spin-current polarization (empty points) as functions of nonadiabaticity parameter.

3(a) for the different V concentrations. The different shapes of depinning boundaries are indicative of modified spin-current polarization and nonadiabaticity parameter with the V concentration.^{12,13,21} In particular we find that the threshold currents are increased with increasing the V concentration.

In order to extract the values of spin-current polarization P and nonadiabaticity parameter β , the depinning boundaries were calculated as functions of β for the various V concentrations using a modified version of the OOMMF code to include the adiabatic and nonadiabatic spin-torque terms.²² The nonadiabaticity parameter β was varied in steps of 0.005 and for each value of β the depinning boundary was calculated, where the starting states used are shown in Fig. 1. For each fixed magnetic field a threshold value u , for which domain-wall depinning occurs, was determined, where $u = JPg\mu_B / (2em_S)$. The variation of the threshold current density J with magnetic field is plotted by setting the value of P to give the best fit to the experimental depinning boundary, for which a fitting coefficient is calculated. Here, the fitting coefficient is proportional to the average distance on the y axis between the points of the simulated and experimental boundaries. The resulting fitting coefficients for the different values of β used in the simulations are shown in

Fig. 3(b) for the three different V concentrations. Since the shapes of the depinning boundaries depend on the value of β , a minimum fitting coefficient is obtained and the best-fit depinning boundaries are shown in Fig. 3(a). Thus, we obtain the values $\beta = 0.04 (\pm 2.5 \times 10^{-3})$, $P = 0.39 (\pm 0.02)$ for Py_{99}V_1 (similar to the values previously found in pure Py, namely, $\beta = 0.04$ and $P = 0.4$);^{12,13} $\beta = 0.046 (\pm 2.5 \times 10^{-3})$, $P = 0.36 (\pm 0.02)$ for $\text{Py}_{97.5}\text{V}_{2.5}$; and $\beta = 0.068 (\pm 2.5 \times 10^{-3})$, $P = 0.31 (\pm 0.02)$ for $\text{Py}_{90}\text{V}_{10}$. These values are also shown in the inset to Fig. 3(a).

Since $\beta = \hbar / J_{ex}\tau_{sf}$,⁶ where J_{ex} is the s - d exchange interaction energy and τ_{sf} is the spin-flip time, the increased values of β may arise due to a decrease in either exchange energy or spin-flip lifetime. We know from the variation of A that there is a drop in exchange energy when x is changed from 0 to 10. However, we have also measured the resistivity of these materials and found it to increase with the V concentration, namely, $71.97 \mu\Omega \text{ cm}$ for Py_{99}V_1 , $74.53 \mu\Omega \text{ cm}$ for $\text{Py}_{97.5}\text{V}_{2.5}$, and $83.37 \mu\Omega \text{ cm}$ for $\text{Py}_{90}\text{V}_{10}$ (to be compared with $64.92 \mu\Omega \text{ cm}$ for undoped Py). By increasing the V concentration, the density of scattering centers is increased, resulting in a shortened momentum scattering lifetime, leading to a higher resistivity and, presumably, decreased spin-flip lifetimes by at least the same proportion.

Korringa-Kohn-Rostoker theory calculations show that there is a significant local density of states at a V impurity in Ni associated with virtual bound states. These give rise to a local moment of $\sim 0.5\mu_B$, which is oppositely directed to the magnetization of the Ni host, while an additional reduction in moment of nearby atoms reduces m_S by a total of $\sim 4.5\mu_B/V$ atom.²³ Hence, while pure Ni is a strong ferromagnet, V-doped Ni is weak. We can expect similar physics to take place in Py, which is also a strong ferromagnet. The strongest scattering of transport electrons by a V impurity atom will therefore be of the majority-spin electrons, which are s -like at the Fermi level in undoped Py, into these virtual bound states created near the impurity sites, leading to a particularly strongly enhanced resistivity in the spin- \uparrow channel,²⁴ which will reduce the polarization P of the current.

While a great deal is known about these transport properties in such dilute alloys in the low-temperature limit, reviewed by Mertig,²⁵ the picture concerning spin-flip scattering is less clear as it typically arises from inelastic scattering. Nevertheless, it is reasonable to expect that the rise in the overall momentum scattering rate $1/\tau_k \propto \rho$ that we see from the resistivity measurements will lead to at least a proportional rise in the spin-flip scattering rate $1/\tau_{sf}$, enhancing β . We may expect an increase in the probability of any given scattering event being a spin-flip one from the finite-temperature fluctuations of the local moments on the V sites, causing a further increase in β .

Experimentally, the resistivity in Py films has been found to be proportional to α as a function of thickness,²⁶ but in other cases it was found that the increase in resistivity does not necessarily lead to an increase in damping.²⁷ For the present case of V-doped Py films with fixed thickness we find that the increase in material resistivity with V concentration leads to a clear increase in β , while very little effect is observed on the magnetization damping. This leads us to

conclude that β arises from a different microscopic mechanism to α in these materials. In a recent study of Ho-doped Py nanowires,²⁸ where α shows a strong dependence on Ho doping, it was found that β also increases with the dopant concentration. The authors concluded that in Ho-doped Py the spin relaxation that leads to nonadiabatic spin torque originates from the same mechanism as the angular momentum dissipation that causes damping.²⁸ We hope that these results will stimulate further theoretical investigations into the relationship between nonadiabatic spin torque and damping.

Finally, we note that even though the nonadiabatic spin-torque term has an increasing contribution as the V concentration is increased, the overall threshold current values are larger. We can see that in the expression for u , both spin-transfer torques are proportional to the ratio P/m_S , and so this is due to the drop in spin-current polarization P , due to the increased scattering of majority-spin carriers as described above, being larger than the corresponding drop in m_S , resulting in a proportional decrease in both the adiabatic and nonadiabatic spin-torque terms.

In summary, we have measured the nonadiabaticity pa-

rameter and spin-current polarization in V-doped Py nanowires. By increasing the V concentration we have shown that the nonadiabaticity parameter β is increased due to both the drop in exchange energy and the increasing density of scattering centers resulting in shortened spin-flip times. However, the Gilbert damping α is unaffected by the increase in the V concentration, indicating that these two parameters representing dissipative processes do not reflect the same underlying microscopic mechanisms. On the other hand, increasing the V concentration lowers the spin-current polarization more rapidly than the magnetization, resulting in overall increased threshold currents, in spite of higher values of β .

This research was supported by the ESF EUROCORES collaborative research project SpinCurrent under the Fundamentals of Nanoelectronics program, and by the EPSRC through the Spin@RT consortium. We are grateful to the Diamond Light Source for the provision of beamtime. We would like to thank David Edwards for the suggestion of using V as a dopant.

-
- ¹C. H. Marrows, *Adv. Phys.* **54**, 585 (2005).
²S. S. P. Parkin, M. Hayashi, and L. Thomas, *Science* **320**, 190 (2008).
³G. Tatara and H. Kohno, *Phys. Rev. Lett.* **92**, 086601 (2004).
⁴Z. Li and S. Zhang, *Phys. Rev. B* **70**, 024417 (2004).
⁵S. Zhang and Z. Li, *Phys. Rev. Lett.* **93**, 127204 (2004).
⁶A. Thiaville, Y. Nakatani, J. Miltat, and Y. Suzuki, *EPL* **69**, 990 (2005).
⁷L. Heyne, M. Kläui, D. Backes, T. A. Moore, S. Krzyk, U. Rüdiger, L. J. Heyderman, A. Fraile Rodríguez, F. Nolting, T. O. Menten, M. Á. Niño, A. Locatelli, K. Kirsch, and R. Mattheis, *Phys. Rev. Lett.* **100**, 066603 (2008).
⁸E. Martinez, L. Lopez-Diaz, O. Alejos, L. Torres, and C. Tristan, *Phys. Rev. Lett.* **98**, 267202 (2007).
⁹M. Hayashi, L. Thomas, C. Rettner, R. Moriya, Y. B. Bazaliy, and S. S. P. Parkin, *Phys. Rev. Lett.* **98**, 037204 (2007).
¹⁰H. Kohno, G. Tatara, and J. Shibata, *J. Phys. Soc. Jpn.* **75**, 113706 (2006).
¹¹Y. Tserkovnyak, H. J. Skadsem, A. Brataas, and G. E. W. Bauer, *Phys. Rev. B* **74**, 144405 (2006).
¹²S. Lepadatu, M. C. Hickey, A. Potenza, H. Marchetto, T. R. Charlton, S. Langridge, S. S. Dhesi, and C. H. Marrows, *Phys. Rev. B* **79**, 094402 (2009).
¹³S. Lepadatu, A. Vanhaverbeke, D. Atkinson, R. Allenspach, and C. H. Marrows, *Phys. Rev. Lett.* **102**, 127203 (2009).
¹⁴I. M. Miron, P.-J. Zermatten, G. Gaudin, S. Auffret, B. Rodmacq, and A. Schuhl, *Phys. Rev. Lett.* **102**, 137202 (2009).
¹⁵J. O. Rantschler, R. D. McMichael, A. Castillo, A. J. Shapiro, W. F. Egelhoff, Jr., B. B. Maranville, D. Pulugurtha, A. P. Chen, and L. M. Connors, *J. Appl. Phys.* **101**, 033911 (2007).
¹⁶S. Chikazumi, *Physics of Ferromagnetism* (Oxford University Press, Oxford, 1998).
¹⁷F. Acker and R. Huguenin, *J. Phys. F: Met. Phys.* **6**, L147 (1976); *J. Magn. Magn. Mater.* **12**, 58 (1979).
¹⁸P. S. Keatley, V. V. Kruglyak, A. Neudert, M. Delchini, R. J. Hicken, J. R. Childress, and J. A. Katine, *J. Appl. Phys.* **105**, 07D308 (2009).
¹⁹P. S. Keatley, V. V. Kruglyak, A. Neudert, E. A. Galaktionov, R. J. Hicken, J. R. Childress, and J. A. Katine, *Phys. Rev. B* **78**, 214412 (2008).
²⁰M. J. Donahue and D. G. Porter, NIST Interagency Report No. 6376, 1999; <http://math.nist.gov/oommf>
²¹J. He, Z. Li, and S. Zhang, *J. Appl. Phys.* **98**, 016108 (2005).
²²A. Vanhaverbeke, <http://www.zurich.ibm.com/st/magnetism/spintevolve.html>
²³N. Stefanou, A. Oswald, R. Zeller, and P. H. Dederichs, *Phys. Rev. B* **35**, 6911 (1987).
²⁴I. Mertig, R. Zeller, and P. H. Dederichs, *Phys. Rev. B* **47**, 16178 (1993).
²⁵I. Mertig, *Rep. Prog. Phys.* **62**, 237 (1999).
²⁶S. Ingvarsson, L. Ritchie, X. Y. Liu, G. Xiao, J. C. Slonczewski, P. L. Trouilloud, and R. H. Koch, *Phys. Rev. B* **66**, 214416 (2002).
²⁷G. Council, T. Devolder, J.-V. Kim, P. Crozat, C. Chappert, S. Zoll, and R. Fournel, *IEEE Trans. Magn.* **42**, 3323 (2006).
²⁸T. A. Moore, M. Kläui, L. Heyne, P. Möhrke, D. Backes, J. Rhensius, U. Rüdiger, L. J. Heyderman, J.-U. Thiele, G. Woltersdorf, C. H. Back, A. Fraile Rodríguez, F. Nolting, T. O. Menten, M. Á. Niño, A. Locatelli, A. Potenza, H. Marchetto, S. Cavill, and S. S. Dhesi, *Phys. Rev. B* **80**, 132403 (2009).